Comparative study of dye adsorption onto CNT/PVDF and reduced rGO/PVDF membranes post-treated by a swelling and freeze-drying process

Nianzi Sui, Guanglin Wang, Yangyang Huan, Guangfen Li*, Chaoqun Hao, Wei Chen

State Key Laboratory of Separation Membranes and Membrane Processes, School of Materials Science and Engineering, TianGong University, Tianjin 300387, China, Tel. +86 22 83955074; Fax: +86 22 83955055; emails: liguangfen@tjpu.edu.cn (G. Li), 1291359494@qq.com (N. Sui), 294736581@qq.com (G. Wang), 1547673352@qq.com (Y. Huan), 1781585747@qq.com (C. Hao), 773732656@qq.com (W. Chen)

ABSTRACT

Multi-walled carbon nanotube or reduced graphene oxide were incorporated into polyvinylidene fluoride (PVDF) for constructing porous polymer membranes, which were post-treated by a swelling and freeze-drying process for controlling the type and amount of pore structures. A solvent/non-solvent system as N,N-dimethylformamide (DMF)/water solution was used to swell the as-prepared membranes; afterward, the swollen membranes were frozen in liquid nitrogen. The effects of DMF content in the solution, swelling time and freezing time on the crystallization properties, membrane morphology, hydrophobicity, dye adsorption capacity and mechanical performances were comprehensively investigated by X-ray diffraction, field-emission scanning electron microscopy, the contact angle analysis, the ultraviolet spectroscopy and so on. The scanning electron microscope observation showed that the process conditions of the PVDF blend membrane have dominant effects on the pore's structure. For membranes treated with increasing content of DMF, the surface morphology becomes dense and the cross-section morphologies change from finger-like structure to sponge-like structure. The content of the swell agent indeed has remarkable impacts on the cross-section structure. Despite similar hydrophilicity and mechanical properties are found in two types of membranes, higher adsorption properties for methylene blue dyes were found in carbon nanotubes (CNT/PVDF) membranes. The studies of adsorption kinetics and isothermal suggest that the adsorption process of CNT-based membranes is more consistent with the Freundlich isotherm model and fitted with a pseudo-first-order model.

Keywords: Multi-walled carbon nanotube; Reduced graphene oxide; Poly(vinylidene fluoride); Swelling; Freeze-drying

1. Introduction

Recently, the widespread use of dyes has led to serious water pollution. Dyes are water-soluble organic substances and have an affinity to the applied materials like fabric, thus produce a bright and permanent color [1]. They have found a lot of applications in the fields, especially in the textile industry. In the production process of colored dyes, a large amount of toxic and harmful substances such as aromatic and polycyclic aromatics are transferred to the water. Cyclic compounds that exist in water can have an impact on human health. Dyes can residue in the environment for a long time, and high concentration and stability cause wastewater to be difficult to handle and not easily degraded [2]. Therefore, the treatment of industrial dye wastewater has become a hot topic.

* Corresponding author.

The removal of dyes from the wastewater can take various physical, chemical and biological methods, for example, agglomeration, ion exchange, ultrafiltration, dialysis, chemical oxidation, electrochemical processes [3] and photodegradation [4,5]. However, these methods are only effective and economically advantageous at high concentrations and have the disadvantage of the opposite energy consumption, which may also produce large amounts of toxic or carcinogenic by-products. Currently, adsorption has proved to be an attractive method of removing dyes from wastewater due to economic benefits and low operating costs. In the past few decades, many studies have reported the removal of heavy metal ions and organic dyes by using activated carbon natural minerals, and nanomaterials as adsorbents [6].

Among various nanomaterials, carbon nanotubes and graphene oxide were regarded as ideal nanofillers for polymeric ultrafiltration membranes as they could provide excellent performance in thermal, electrical, mechanical and other aspects [7,8]. Since its first discovery in 1991 [9,10] it has been used in various fields such as hydrogen storage, [11] catalysis [12] and drug delivery. In addition, due to its excellent structural characteristics and high surface area, carbon nanotube (CNT) is also used as an adsorbent to remove heavy metal ions such as Mn^{+7} in industrial wastewater [13]. Compared with common adsorbents such as activated carbon, it has been found that carbon nanotubes exhibit higher removal efficiency of heavy metal ions and dyes in wastewater. Graphene oxide also is an adsorbent owing to its large surface area and a large number of oxygen-containing functional groups, such as carboxyl, hydroxyl, and epoxide [14]. Gao et al. [15] used graphene oxide (GO) as an excellent sorbent to remove tetracycline. However, the poor dispersion of CNTs and GO in solvent and polymer has restricted its application. Therefore, some tactics were taken by surface-modified such as carboxylation and hydroxylation to improve their hydrophilicity and the dispersion of CNTs and replaced GO with reduced graphene oxide (rGO) in the polymer membranes. Therefore, the simple method of improving the adsorption performance of polymers by using functionalized CNT-polymer blended porous membranes is very desirable [16].

In addition to the adsorption of nanoparticles, ultrafiltration membranes have also been widely used in wastewater treatment and dyes adsorption processes in recent years. Among them, polyvinylidene fluoride (PVDF) has become one of the most popular ultrafiltration membrane materials [17,18]. This is because PVDF easily dissolves in common organic solvents and can be produced via a simple immersion precipitation phase separation process. PVDF is advantageous over other membrane materials due to its strong maneuverability, excellent mechanical properties, thermal properties, chemical resistance, and thermodynamic compatibility with other polymers. However, the PVDF materials are easily fouled due to their hydrophobicity. Many efforts have been made in improving the hydrophilicity and anti-fouling performance by different methods such as surface coating, [19] the addition of hydrophilic additives [20] and inorganic nanomaterials [21,22]. Zhao et al. [23] fabricated the PVDF/GO ultrafiltration membranes for Sewage treatment. They found that this ultrafiltration membrane has better hydrophilicity, permeability and antifouling properties. Safarpour et al. [24] prepared the rGO/TiO$_2$/PVDF membranes that showed better hydrophilicity, higher pure water flux and reject rate than the original PVDF. Zhang et al. [25] modified the PVDF membrane with the multi-walled carbon nanotube (MWCNT) and found that due to the addition of carbon nanotubes, the hydrophilicity, pure water flux, membrane pore distribution and mechanical strength of hybrid membranes have changed significantly. These studies revealed that the morphology of the membrane pores has predominated effect on the membrane properties and adsorption capacity for dyes. For a better controlling membrane surface morphology, a few studies have been carried out by using polystyrene and nature polymer composites. Liang et al. [26] prepared PS porous membrane material by solvent/non-solvent swelling and liquid nitrogen freezing two-step method. It was found that the pore structure can be controlled by adjusting different swelling times and freezing times. Liu et al. [27] prepared chitosan/xanthan/montmorillonite nanocomposites into a gel structure by freezing. The results show that different freezing modes affect the formation of porous structures and the hardness of porous membranes.

In this study, using the swelling and freeze-drying method to modify MWCNTs/PVDF and rGO/PVDF blended membranes which were prepared by the phase inversion method [26,27]. We chose N,N-dimethylformamide (DMF)/water system as the swelling agent and freeze-drying with liquid nitrogen. The effects of swelling time and freezing time in the membrane formation process on the crystallization and membrane hydrophilicity were discussed by X-ray diffraction (XRD) and contact angle measurement. The adsorption performance of the different types of hybrid membranes in methylene blue (MB) solution was analyzed by a UV spectrophotometer. In addition, the surface and cross-section morphology of membranes were imaged by field-emission scanning electron microscopy (FE-SEM) and single fiber electronic tensile strength tester to confirm the mechanical properties of resulted porous membrane materials.

2. Experimental

2.1. Materials

PVDF asymmetric flat membrane was prepared by dissolving powdered polyvinylidene fluoride (PVDF, M_w = 450 kDa, Arkema Inc.) in N,N-dimethylformamide (DMF ≥99.5% Tianjin Kermel Chemical Reagents Co., Ltd., Tianjin, China). Carboxylated multi-walled carbon nanotubes (MWCNT-COOH, carboxyl content 0.49 wt.%, length 10–20 μm, purity >98 wt.%, Chengdu Organic Chemistry Co., Ltd., China), and reduction of graphene oxide (rGO, purity >99 wt.%, Chengdu Organic Chemistry Co., Ltd., China) was used as received. Liquid nitrogen (99.99% purity) was purchased from Tianjin HuanYu Gas Company. Anhydrous ethanol (99.7%) was obtained from Tianjin WindShip Chemical Technology Co., Ltd., China. Methylene

blue (MB, M_w = 373.9) was purchased from Tianjin Guangfu Chemical Research Institute, China.

2.2. Preparation of CNT (rGO)/PVDF blend membranes

0.05 g MWCNTs or rGO was dispersed in 30 mL DMF and ultrasonicated for 60 min until achieving a uniform dispersion. 5 g PVDF powder was dried at 60°C for 2 h prior to use and then dissolved in above dispersion at 70°C for approximately 5 h to form a homogeneous casting solution, which was then cooled down and stored at vacuum drying oven for 8 h to remove the bubbles through the vacuum environment. The CNT/PVDF and rGO/PVDF blended membranes were prepared by phase inversion. The degassed casting solution was cast onto a glass plate via a rod with a thickness of 300 μm to form a membrane, which was then immersed into a deionized (DI) water coagulation bath at RT for water/DMF exchange. After coagulation, the membranes were transferred to a fresh DI water bath and steeped for 48 h to remove residual solvent from the film. In the end, the membranes were dried in air at RT (298 K) for further use.

2.3. Process of swelling and freeze-drying

To optimize the experimental conditions for obtaining controllable porous PVDF blended membranes, the above membranes were immersed in a DMF/H$_2$O solution and swollen for 5, 10 and 15 min, and then frozen in liquid nitrogen for 0.5, 1 and 1.5 h. The DMF/H$_2$O solution has a concentration from 4, 8 to 12 wt.%. A porous hybrid membrane is obtained after being taken out of liquid nitrogen and dried in air. The process of swelling and freeze-drying is shown in Fig. 1. The influences of DMF content in the solution, swelling time and freezing time on the morphologies and surface properties of PVDF blended membrane were extensively investigated by SEM and goniometer. The related experimental parameters such as the content of DMF in water, swelling time and freezing time are shown

in Table 1. The samples of PVDF containing CNT or rGO were named Cn and Rn, respectively.

2.4. Characterization

Wide-angle X-ray diffraction is a common method to measure the crystalline structure and polymorphism of polymeric nanocomposites. The analysis was performed in wide-angle X-ray diffraction (XRD, D8 ADVANCE, Bruker) operating at 40 kV, 40 mA with Cu Kα radiation (λ = 0.154 nm) [28]. All membranes were detected in a continuous scan range from 10° to 45° of 2θ. The morphologies of the surface and cross-section of membranes
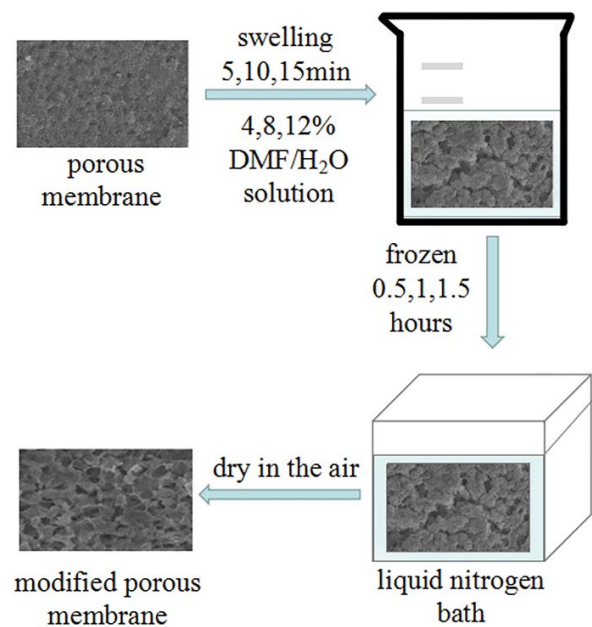

Fig. 1. Process of swelling and freeze-drying.

Table 1
Table for varying three experimental parameters as content of DMF in water, swelling time and freezing time

Sample ID (C_i, R_i)		DMF/H$_2$O (wt.%)[a]	Swelling time (min)[b]	Freezing time (h)[c]
C1	R1	4	5	0.5
C2	R2	4	10	1
C3	R3	4	15	1.5
C4	R4	8	5	1
C5	R5	8	10	1.5
C6	R6	8	15	0.5
C7	R7	12	5	1.5
C8	R8	12	10	0.5
C9	R9	12	15	1

C_i is MWCNT modified membrane; R_i is rGO modified membrane (*i* represents different processing conditions).
[a]DMF/H$_2$O (wt.%): represents DMF accounts for a few percent of DMF/H$_2$O's mass;
[b]Swelling time (min): corresponds to the time of the hybrid membrane in the DMF/H$_2$O swelling agent;
[c]Freezing time (h): corresponds to the time of the hybrid membrane in liquid nitrogen.

were observed by using field-emission scanning electron microscopy (FE-SEM, Hitachi s-4800, Hitachi Limited, Japan). The water contact angle of the membranes was measured by a contact angle tester (DSA-100, Kruss, Germany). Each group was measured 10 times and averaged as the final water contact angle.

2.5. Adsorption experiments

To determine the adsorption performance of the prepared membranes, cut the membranes into small pieces of 1 cm × 2 cm, and then immersed into 30 mL MB solution with appropriate concentration, which ranged from 0, 5, 10, 20, to 30 mg/L. The absorbance of the samples was recorded at 663 nm using a UV-Vis spectrophotometer (PerkinElmer Ultraviolet-35, USA) to determine the residual substrate concentration. Each experiment was repeated three times, and the mean value was taken to represent the experimental data. The adsorption capacity, Q_t was calculated according to Eq. (1) [29]:

$$Q_t = \frac{(C_0 - C_t) \times V}{m} \tag{1}$$

where Q_t is the amount of methylene blue adsorbed on blend membranes (mg/g), C_0 is the initial concentration of MB (mg/L), C_t is the instantaneous concentration of MB at time t (mg/L), V is the volume of the solution (L), and m is blend membrane quality (g).

To specifically study the adsorption rate of the composite membrane and the time to reach the equilibrium adsorption, we fit the kinetic model of the MB adsorption process of the composite membrane, including pseudo-first-order and pseudo-second-order models. The kinetic model is as follows [6]:

$$Q_t = Q_e \left(1 - e^{-K_1 t}\right) \tag{2}$$

$$Q_t = \frac{K_2 Q_e^2 t}{1 + K_2 Q_e t} \tag{3}$$

where, Q_t (mg/g) is the adsorption amount of MB corresponding to the blend membrane at different times, and Q_e (mg/g) is the adsorption amount at equilibrium. K_1 (min⁻¹) and K_2 (g mg⁻¹ min⁻¹) are the rate constants for adsorption kinetics.

3. Results and discussion

3.1. XRD spectra of membrane characterization

PVDF is well known to crystallize in several crystal polymorphs (α, β, and γ), depending on processing conditions such as the solvent used, temperature, and polymerization [30,31]. Fig. 2 shows crystallization behavior of CNT/PVDF and rGO/PVDF blend membrane after being treated by swelling and freeze-drying process. It can be seen that several discernable diffraction peaks appear at 18.4°, 26.3° and 36.2°, which are corresponding with the α-phase. The diffraction peak at 20.4° is the β-phase of PVDF. Fig. 2c appears a strong and sharp diffraction peak of β, and a weak diffraction peak of α. The increasing DMF, content is insufficient in allowing the PVDF molecular chain rearrangement during a short freezing time and only part of the α-phase translates into the β-phase. The hybrid membrane is composed of a number of crystalline particulates. However, in rGO/PVDF blend membrane, these two diffraction peaks had a tendency to decrease randomly, as shown in Fig. 2d–f, because the presence of rGO is not conducive to the rearrangement of polymer molecule chains and chains are disrupted during the swelling-freezing process.

3.2. SEM analysis of PVDF/CNT and PVDF/rGO blend membranes

The surface morphology of PVDF/CNT blend membranes was imaged by SEM and shown in Fig. 3. The change of pore structure during the preparation of the membrane was influenced by three experimental parameters as DMF content in water, swelling time and freezing time. First of all, from Fig. 3g–i (C7–C9), due to a high concentration of swelling agent (DMF content accounted for 12%), an improved ability to make it into the membrane, along with the expansion of the swelling time (5–15 min), allowing more DMF molecules into the membrane body and causing swelling of membrane. After freezing treatment, the swelling agent is released evenly which leads to uniformly formed crystallites of PVDF on the surface and no obvious pore structure was observed. The results show that high swelling time and DMF content are not conducive to the formation of pore structure. Further, in Fig. 3a (C1), b (C2) and d–f (C4–C6), the pore structure can be clearly seen, especially in Fig. 3a and b. This again indicates that low DMF content is contributed to the formation of the surface pore. However, the pore structure in Fig. 3c (C3) and g (C7) is not obvious, and the network structure appears, which is because the long freezing time (1.5 h) is not conducive to the formation of the pore structure of the sample. In summary, low DMF content plays a key role in the formation of pore structure. High swelling time and freezing time do not help for the formation of pore structure.

Fig. 4 shows that the cross-section morphology of the membranes treated by the swelling and freeze-drying method. All the membranes contain typical two structures as finger-like structures near the surface and sponge-like structures near the bottom surface. Obviously, from Fig. 4a–f, it can be concluded that a low DMF content is conducive to the formation of finger-like pores, while a high DMF content (12 wt.% DMF/H$_2$O) from Fig. 4g–i, resulting in a reduction in finger-like pores, an increase in sponge-like pores and a decrease in the size of the pores [26]. This is because, with the increase of DMF content, it is beneficial for DMF to enter the inside of the membrane. The more content of DMF slows the exchange rate of solvent and non-solvent and extends phase separation progress, which eventually leads to the decreases of the finger-like structure and formation of dense sponge-like pores. The swelling time was used to control the amount of DMF taken into membranes, whereas the freezing time was for controlling the release of DMF. When the DMF content was certain, it could be clearly observed from Fig. 4a–c
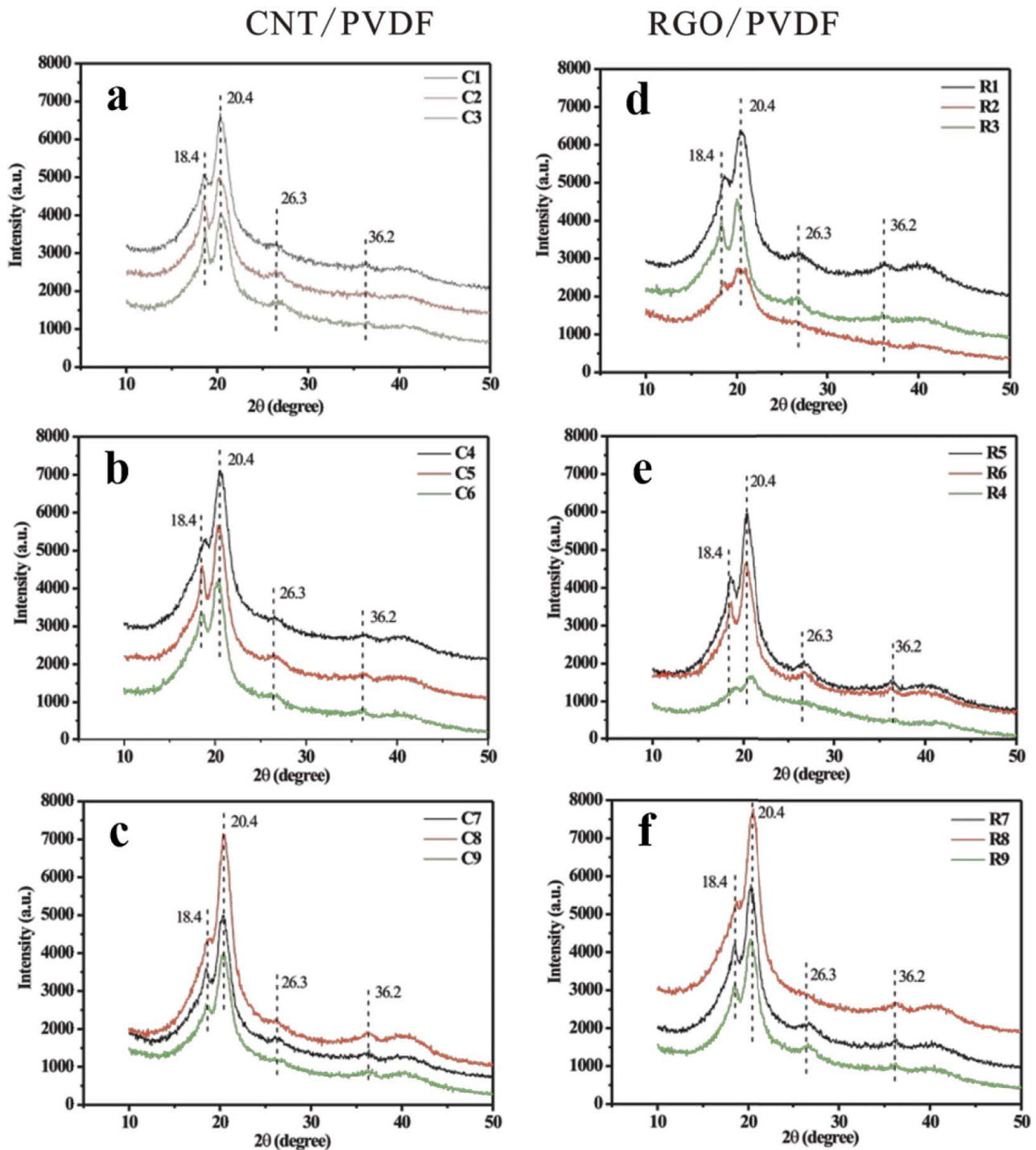
Fig. 2. A comparison of XRD patterns of MWCNT/PVDF (a–c) and rGO/PVDF (d–f) membranes treated under different content of DMF, swelling time and freezing time.

(4 wt.% DMF/H_2O, C1–C3) and Fig. 4d–f (8 wt.% DMF/ H_2O, C4–C6) that the number of finger-like pores in Fig. 4b and e was more than that of other samples in the same group. This is due to low swelling time limits DMF content entering the membrane, so the number of finger-like pores is limited (Fig. 4a and d), while high swelling time makes the amount of DMF enter the membrane body more,

but the limited freezing time (0.5–1.5 h) is not enough for the complete release of DMF, thus there are relatively few finger-like pores. When the swelling time is 10 min, Fig. 4b (freezing time 1 h) and 4e (freezing time 1.5 h) fully release the DMF contained in the membrane, so their finger-like pores are more than other samples in the same group [26]. Therefore, suitable swelling time and freezing time is the
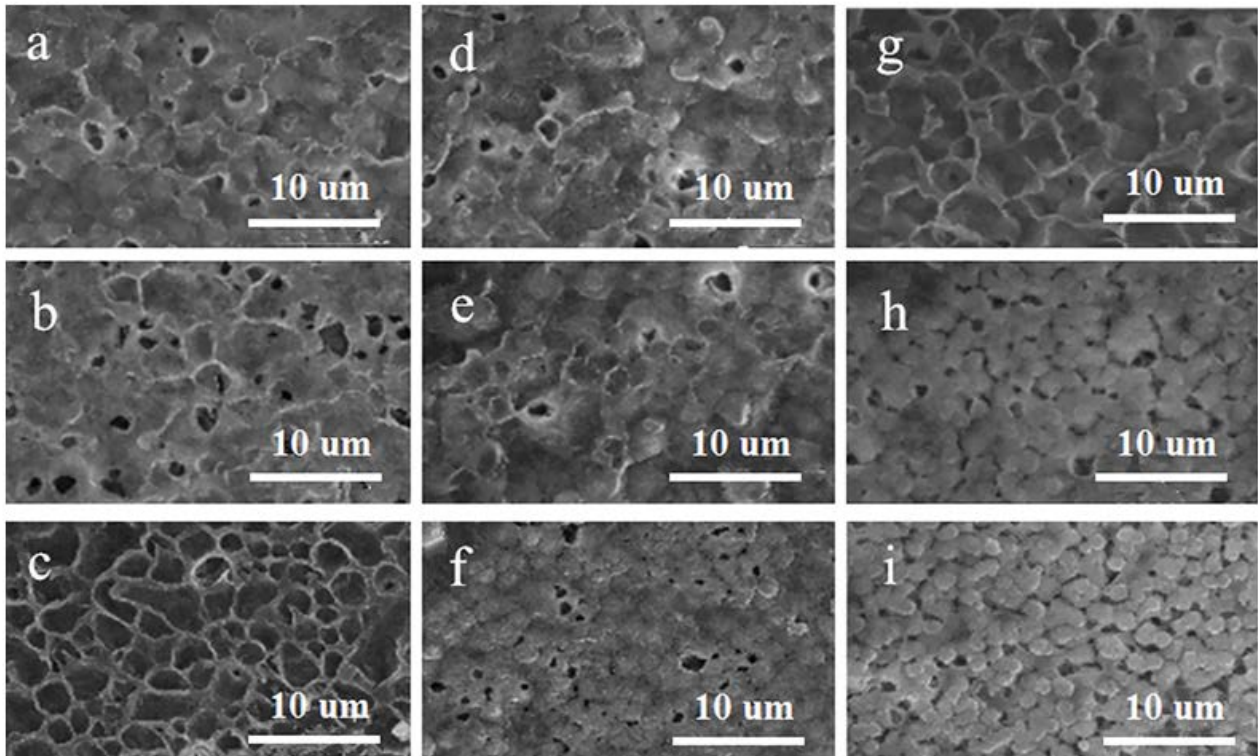
Fig. 3. SEM analysis of the PVDF/CNT membrane tuning by different swelling and freezing time, (a) C1, (b) C2, (c) C3, (d) C4, (e) C5, (f) C6, (g) C7, (h) C8, and (i) C9.
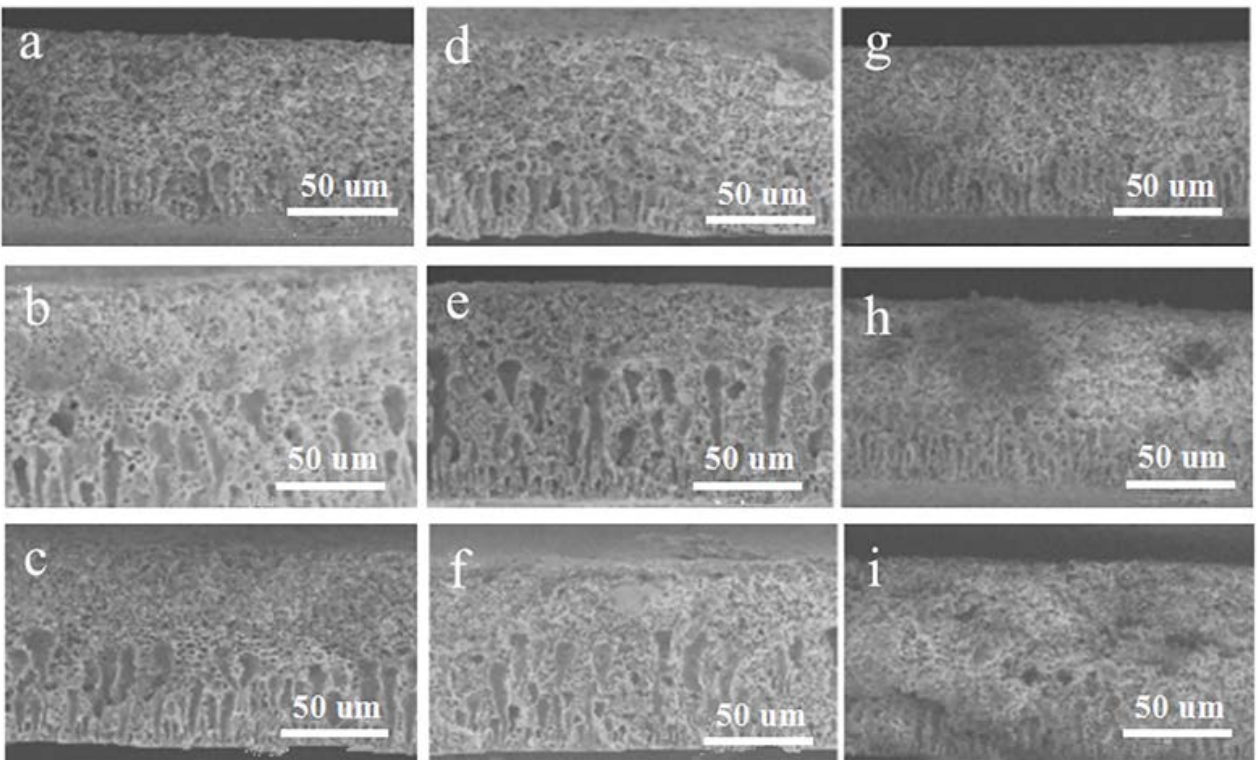
Fig. 4. SEM analysis of the cross-section for PVDF/CNT membrane tuning by different DMF content, swelling and freezing time, (a) C1, (b) C2, (c) C3, (d) C4, (e) C5, (f) C6, (g) C7, (h) C8, and (i) C9.

key to obtain more finger pores. A low DMF content contributes to the formation of the finger-like pore.

Comparing with PVDF/CNT membranes, different surface morphologies were observed on the PVDF/rGO membranes, as shown in Fig. 5. For membranes treated with DMF content below 12 wt.%, regular and uniform network-like structures were found on the membrane surfaces (Fig. 5a–f). The same morphology is also found for the membrane treated with a DMF content of 12 wt.% and lower swelling time (Fig. 5g). The reason is that the swelling of membranes in DMF/water mixture can cause the rearrangement of rGO molecules in the PVDF matrix, but the rearrangements of two-dimensional rGO on the surface can hardly be achieved during insufficient swelling and freezing time. rGO molecules are vertically aligned on the membrane surfaces, instead of horizontal on the surface, the polymer molecules aggregate around it and form network-like structures. As the DMF content increases up to 12 wt.%, the network structure disappears and a few unordered pores are located on the membrane surface, which becomes much smoother (Fig. 5h and i). This is probably due to both higher DMF content and prolonging swelling time promotes the amount of DMF to enter the membrane and sufficiently swells PVDF molecules that eventually enclosed rGO.

For a better understanding, the effect of experimental conditions on membrane morphologies, the cross-section morphologies of PVDF/rGO membranes can be seen from Fig. 6. For the membrane treated with DMF content below 12 wt.%, the membranes consist of a dense, narrow finger-like structure in the upper layer, a wider and longer finger-like structure in the intermedia layer and a sponge-like structure in the bottom. Either increasing DMF content or extending swelling time, the finger-like structure in the middle area becomes longer and wider (Fig. 6a–f). For membranes treated with higher content of DMF, the cross-section areas are quite similar to that of PVDF/CNT membrane (Fig. 6g–i). Thus, the content of the swell agent indeed has a non-negligible effect on the cross-section structure.

3.3. Contact angle analysis

The surface hydrophilicity was evaluated by water contact angle measurement, as displayed in Fig. 7. For CNT-based membranes, the higher content of DMF favors the decreases of water contact angle, as well, for the rGO based membranes, the increase of DMF content decreases water contact angle. It is due to a lower DMF content make for forming pore structures, the elimination of polymer molecules from the surface, the exposed rGO and CNT on the surface increase surface roughness. The maximum water contact angle of the CNT/PVDF membrane was 90.9° of C3, and the maximum contact angle of the rGO/PVDF membrane was 99.7° of R3. This is because the surface of the membrane becomes rough after being treated by the swelling and freezing method, resulting in an increase in hydrophobicity and water contact angle. The lowest contact angles are C5 and R8, the values are 78.1° and 80.6°,
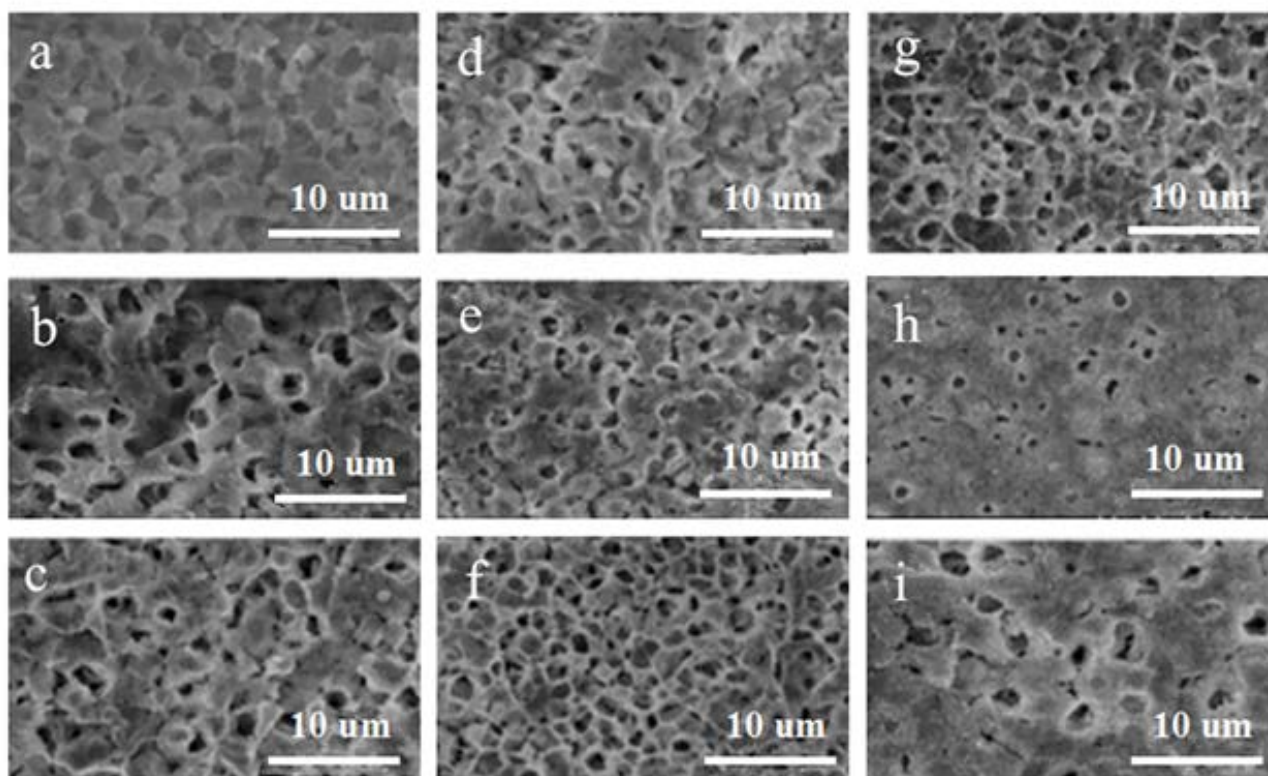

Fig. 5. SEM analysis of the PVDF/rGO membrane tuning by different DMF content, swelling and freezing time, (a) R1, (b) R2, (c) R3, (d) R4, (e) R5, (f) R6, (g) R7, (h) R8, and (i) R9.
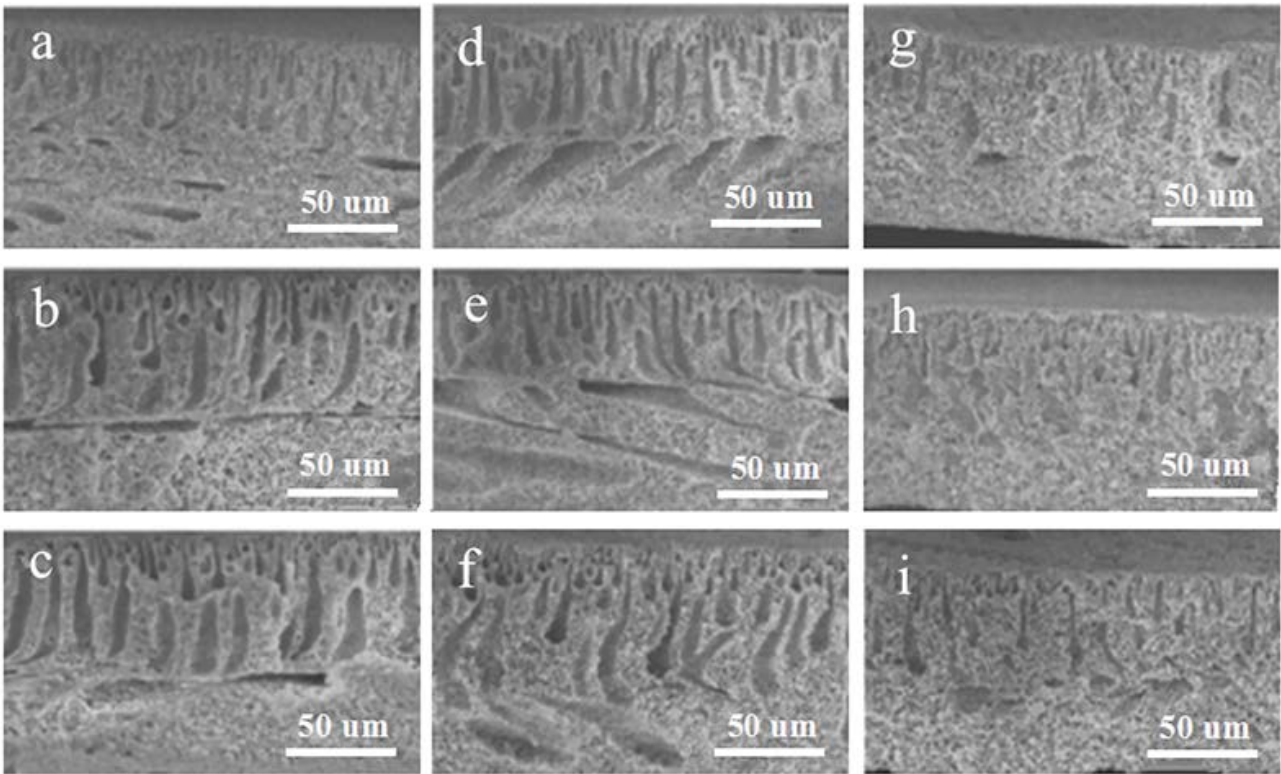
Fig. 6. SEM analysis of the cross-section of PVDF/rGO membrane tuning by different DMF content, swelling and freezing time, (a) R1, (b) R2, (c) R3, (d) R4, (e) R5, (f) R6, (g) R7, (h) R8, and (i) R9.
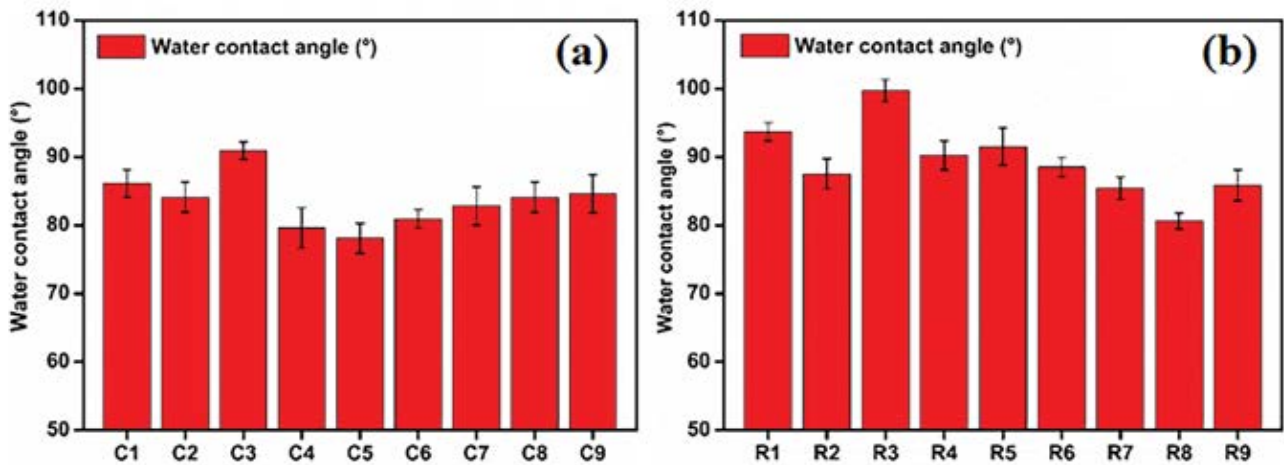

Fig. 7. Water contact angle analysis of the PVDF/CNT (a) and PVDF/rGO (b) blend membranes tuning by different DMF content, swelling and freezing time.

respectively, due to the surface of the sample is relatively smooth and the pore structure is small.

3.4. Mechanical property analysis

The mechanical properties of PVDF blend membranes with either MWCNTs or rGO are shown in Fig. 8. Tensile tests in Fig. 8a show that the weakest tensile strength of

the C1 membrane is about 2.8 MPa, whereas the strongest tensile strength of C9 is about 4.3 MPa. Therefore, when the membranes were swollen in the swelling agent of high concentration for a long time, the molecular chain of the blend membrane performs relaxation and rearrangement, resulting in the collapse of the pores in cross-section and thus enhancing the tensile strength. The corresponding elongation at break of CNT base PVDF membranes varied in the
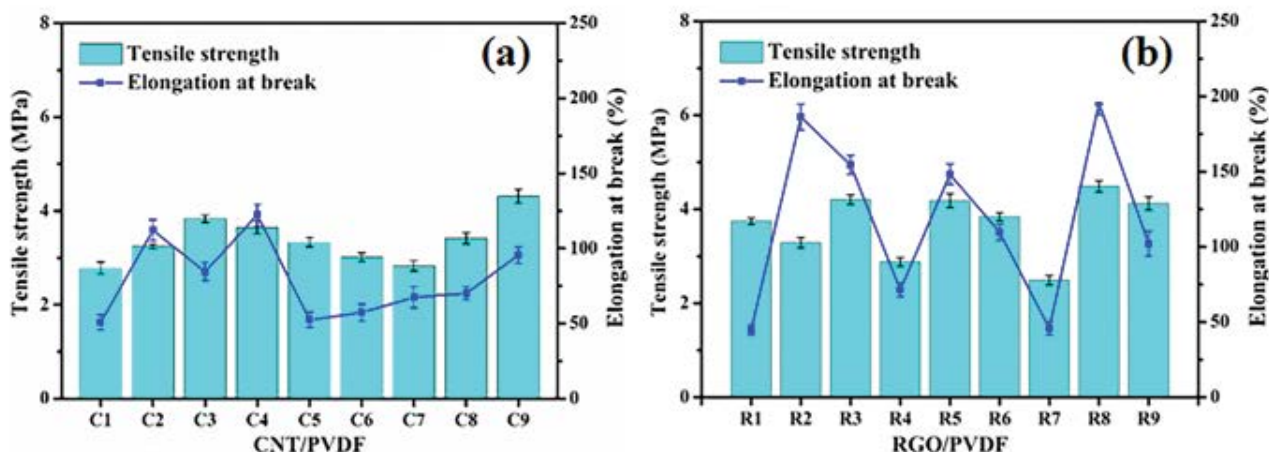
Fig. 8. Comparison of tensile strength and elongation at break of different blend membranes: (a) CNT/PVDF and (b) rGO/PVDF.

range from 50.7% to 122.3%. The strongest tensile strength as 4.5 MPa was found in samples R8, shown in Fig. 8b, which indicates that the content of DMF in the water had undoubtedly effects on the tensile strength of PVDF/rGO blend membranes. The elongations at break of rGO based PVDF membranes were in the range from 45% to 195%. These are attributed to the addition of rGO that improves the elasticity and hardness of the treated blend membranes.

3.5. Adsorption behavior of PVDF/CNT and PVDF/rGO

The adsorption behavior of the blended membrane on MB was investigated using an MB solution at a concentration of 20 mg/L. The adsorption capacity of PVDF/CNT and PVDF/rGO hybrid membranes vs. adsorption time is plotted in Fig. 9. It can be seen that the adsorption capacity of CNT-based PVDF membranes is higher than that of rGO based membranes. Among all these membranes, the highest adsorption capacity was found for the sample of C4 in Fig. 9a. The higher adsorption capacity may attribute to

the co-presence of regular finger-like structure and a large number of loose sponge-like holes in the cross-section of the membrane. Meanwhile, the surface is destroyed by DMF, and the larger surface holes are contributed to dye entering the interior. Whereas, for the rGO based membranes, a higher adsorption capacity was found for samples of R6 and R8, as shown in Fig. 9b. It is probably due to the existence of a lot of holes on the surface and many finger-like structures in the cross-section area, which favors the dye molecular penetrating the membrane. As we can see from Fig. 9, all the membranes experienced quick adsorption of MB in the initial time of 30 min. C4 has the largest adsorption capacity in all membranes, and the adsorption capacity is 1.24 mg/g. Therefore, an appropriate DMF content of 8 mL, a low swelling time of 5 min, and a high freezing time of 1 h are more conducive to the improvement of dye adsorption capacity for CNT/PVDF hybrid membranes.

Table 2 compares the previously reported adsorbents for the MB in the literature and the MB adsorption capacities of the membranes prepared in our study. See that
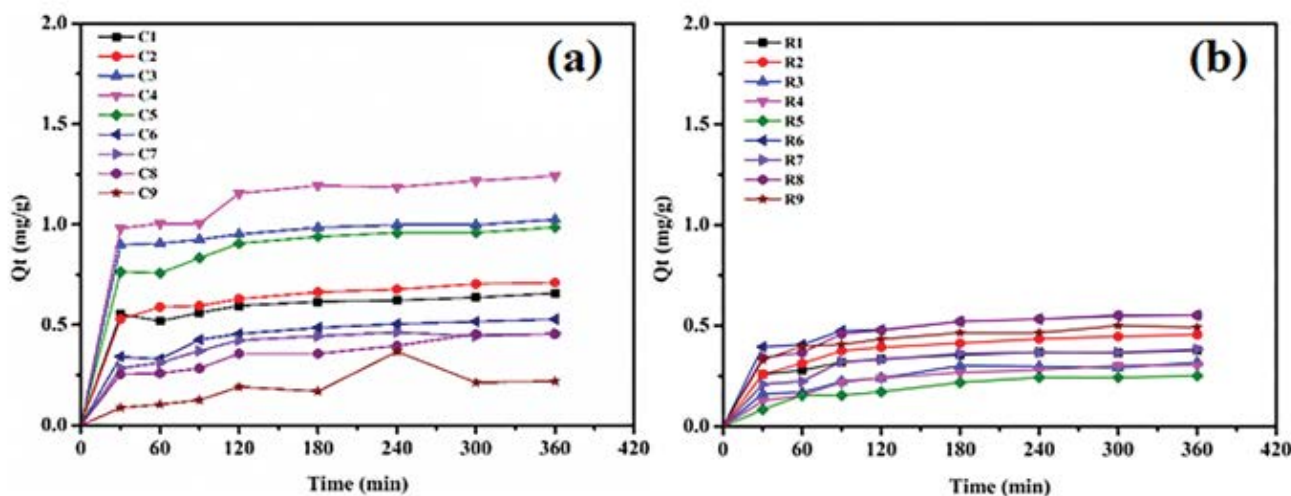

Fig. 9. The adsorption capacity of 20 mg/L MB solution by different types of PVDF/CNT (a), PVDF/rGO (b) blend membranes treated with different content of DMF swelling 5, 10, 15 min.

Table 2
Previously reported adsorption capacities of various adsorbents for methylene blue

Adsorbent	Q_e (mg/g)	Ref.
Indian Rosewood sawdust	11.8–51.4	[32]
Pyrophyllite	70.4	[33]
Jute processing waste	22.5	[34]
Eggshell and eggshell membrane	0.8–0.3	[35]
Activated carbon	435.0	[36]
Carbon nanotubes	35.4–64.7	[37]
AGDPA@AC	159.5	[38]
(ALiCE) pellets	36.25	[39]
Fe_3O_4@AMCA-MIL-53(Al) nanocomposite	30.23	[40]
Carbon nanotubes	124.0	CNT/PVDF in this study
Reduced graphite oxide	60.0	rGO/PVDF in this study

Q_e: the amount of MB adsorbed at equilibrium

this porous membrane for adsorption of dye is in the upper level, and the adsorption amount of MB by equivalent pure CNT and rGO were 124 and 60 mg/g, respectively. The results were significantly higher than those reported before but lower than that of activated carbon. It is indicated that the porous PVDF membrane itself does participate in the adsorption of MB and increases the adsorption capacity by 1 time.

3.6. Adsorption kinetics and isotherms of PVDF/CNT membranes

The adsorption kinetics of the MB solution with different concentrations by the CNT-based membranes were studied through an ultraviolet spectrophotometer. The curves in Fig. 10a clearly show the adsorption of MB by the membrane C4 over time in different concentrations of MB solutions from 5, 10, 20, to 30 mg/L. The value of Q_t for the membrane C4 in MB solution increases significantly in the first 30 min and then reaches a maximum, indicating a rather fast initial adsorption rate of the membrane to MB. It can also be seen that the adsorption amount of MB by the membrane is proportional to the MB solution concentration. When the concentration was 5 mg/L, the adsorption amount of Q_t was 0.2 mg/g, but when the concentration was 30 mg/L, the adsorption amount reached 2.2 mg/g.

For further studying the adsorption process, adsorption isotherms were performed by obtaining the amount of adsorption when it reached equilibrium. Simultaneously, two isotherm models as the Freundlich and Langmuir isotherm models are introduced, as both are the most commonly used models in the field of adsorption to explore the adsorption performance of membranes on MB. By fitting the two isotherm models (Fig. 10b), we obtained a correlation coefficient (R^2) of 0.994 for the Freundlich isotherm model and a correlation coefficient (R^2) of 0.881 for the Langmuir isotherm model. The correlation coefficient of the Freundlich isotherm model is closer to 0.99, which shows that the adsorption process of MB on the membrane is more consistent with the Freundlich isotherm model. This is because the surface of the membrane becomes no longer homogeneous after the swelling and freezing treatment.

And the MB molecules have a positive charge that will repel each other. MB molecules will enter the inside of the membrane from the pores of the membrane surface and fill the pores. The Freundlich isotherm model also verifies that the adsorption of MB on the membrane is not just a monolayer adsorption process. The adsorption amount calculated by the following equation of the Freundlich isotherm model in Eq. (4) is closer to the actual experimental data [6].

$$\ln Q_e = \ln K_F + \frac{1}{n}\ln C_e \tag{4}$$

where Q_e (mg/g) is the equilibrium adsorption amount; C_e (mg/L) is the concentration of MB at equilibrium; K_F ((mg/g)/(L/mg)$^{1/n}$) is the correlation index of the adsorption process; n is the model reaction constant.

Table 3 shows the parameter values of C4 obtained by performing dynamics fitting. We can see that the R^2 of the pseudo-first-order and pseudo-second-order models are 0.999 and 0.989, respectively, which indicating that the adsorption process of the membrane is well fitted with the pseudo-first-order model, which is also proved by Fig. 11. The data obtained from the pseudo-first-order model is basically consistent with the graphs made by the experimental data. From the curve, we can find that the adsorption rate is very fast in the first 30 min of the experiment. This is because the surface of the membrane is not contaminated and the concentration of MB is also high. The adsorption rate gradually decreases after 30 min, which is due to the surface of the membrane has adsorbed more dyes, and the membrane pores are basically occupied by the MB solution, so the adsorption rate of the dye decreases until it reaches the adsorption equilibrium.

3.7. Adsorption mechanism of PVDF/CNT membranes

The cross-section SEM of the PVDF/CNT membrane (C4) after removing dye was shown in Fig. 12a, and it can be clearly observed that spherical impurities embedded in the rich pore structure, which is the MB molecule adsorbed. Further, we carried out energy spectrum scanning (EDS) for
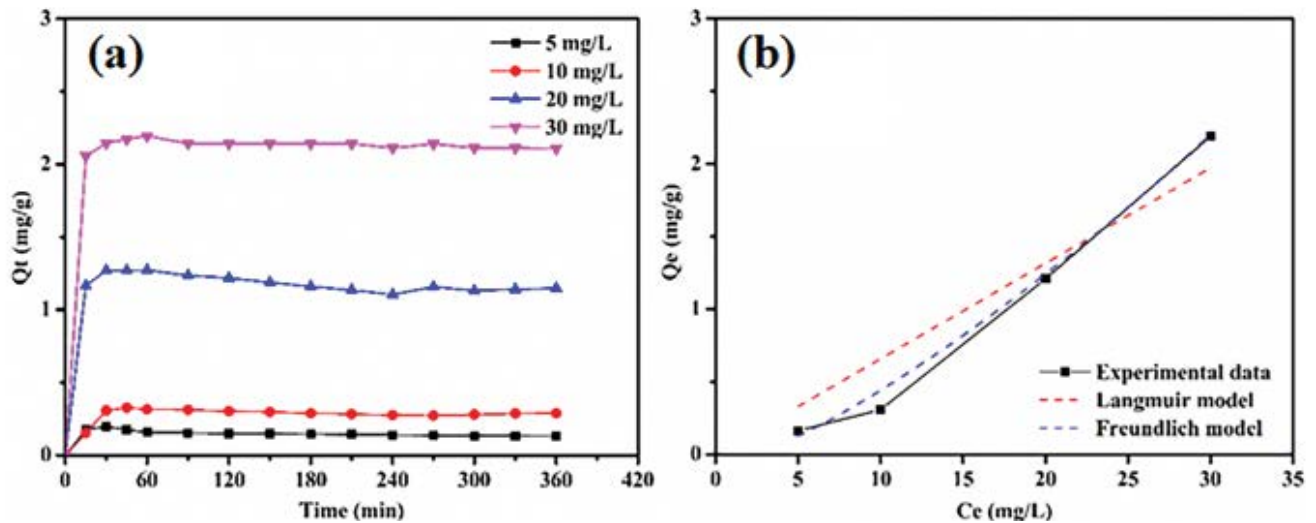
Fig. 10. The adsorption capacity of CNT/PVDF membranes (C4) in different concentrations of MB solutions changes with time (a), and the relationship between the concentration of MB and the amount of adsorption at equilibrium (b).

Table 3
Adsorption kinetics of pseudo-first-order and pseudo-second-order of C4

Model	Parameter	Initial concentration 30 mg/L
Pseudo-first-order	Q_e (mg/g)	2.166
	K_1 (min^{-1})	0.202
	R^2	0.999
Pseudo-second-order	Q_e (mg/g)	2.181
	K_2 (g mg^{-1} min^{-1})	0.617
	R^2	0.989

Q_e: amount of MB adsorbed at equilibrium calculated from pseudo-first-order model or pseudo-second-order model;
K_1: rate constant of the pseudo-first-order kinetic;
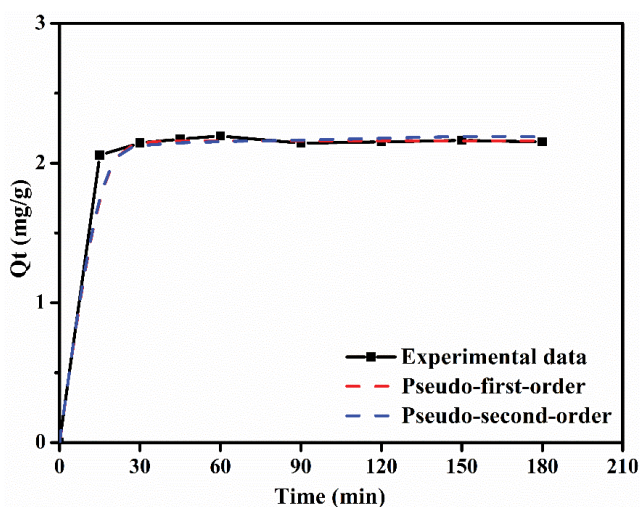K_2: rate constant of pseudo-second-order model;

Fig. 11. The adsorption kinetics fitting curves of pseudo-first-order and pseudo-second-order of CNT/PVDF membranes at different time.

the membrane surface (Fig. 12b), and the results showed that in addition to the original element C/O/F, N and S elements appeared in the sample, which fully demonstrates that molecules were adsorbed on the membrane surface. From its element distribution diagram, it could be concluded that MB was uniformly adsorbed on the membrane surface. This is consistent with Langmuir's model result.

To understand its adsorption for MB, the adsorption mechanism of hybrid membrane was explored. As shown in Fig. 13, the interaction diagram between PVDF/CNT hybrid membrane and MB is visually depicted. Obviously, electrostatic adsorption is one of the ways of interaction between the two, negative groups as hydroxyl and carboxyl existed in CNT easy to adsorb MB (cationic dye). At the same time, hydrogen bonds and pore adsorption also play an important role. Hydrogen bonds exist in oxygen-containing functional groups, fluorine and nitrogen atoms from MB molecules, while pore adsorption is mainly caused by the presence of finger-like and spongy-like holes in the sample, making MB easy to penetrate and be wrapped in it. Furthermore, the benzene ring in the MB molecule interacts with carbon

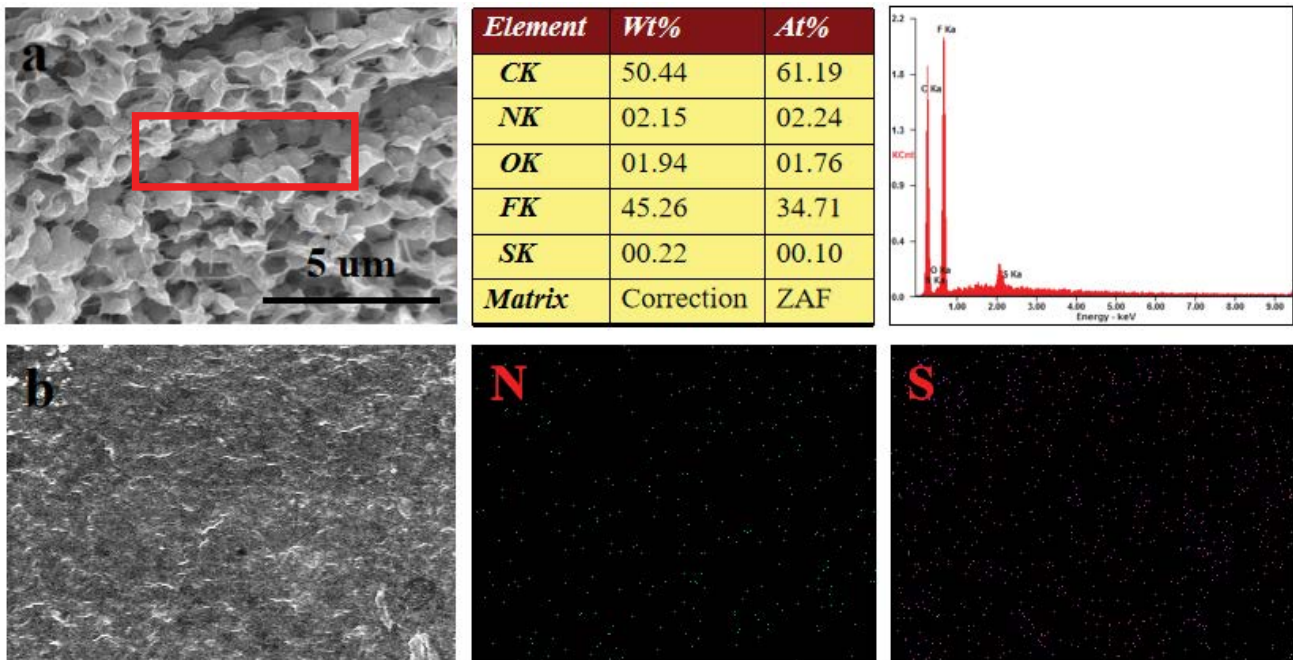| Element	Wt%	At%
CK	50.44	61.19
NK	02.15	02.24
OK	01.94	01.76
FK	45.26	34.71
SK	00.22	00.10
Matrix	Correction	ZAF

Fig. 12. (a) The SEM of the cross-section of PVDF/CNT membrane (C4) after dye removal and the EDS spectrum of membrane surface (b).
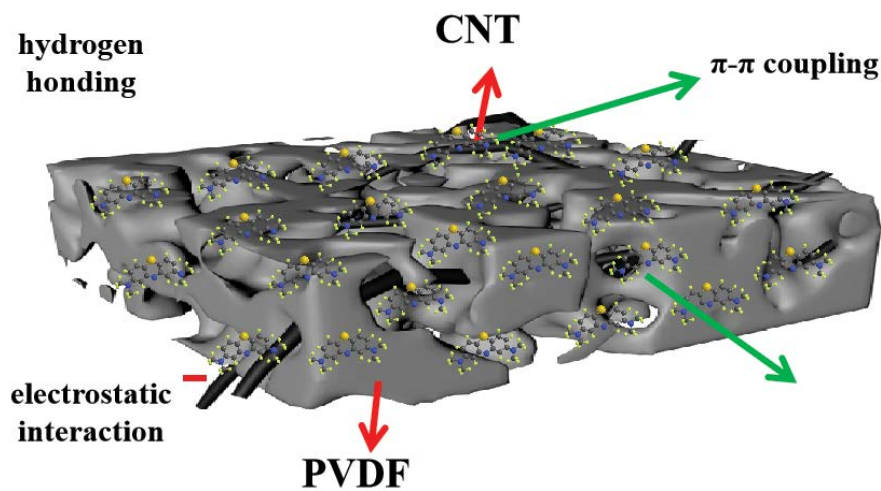

Fig. 13. Adsorption mechanism of MB adsorbed by PVDF/CNT hybrid membranes.

nanotubes embedded in the PVDF matrix via π-π coupling. Therefore, under the above four forces, MB molecules were adsorbed on the surface and pore structure of the CNT/PVDF hybrid membrane.

4. Conclusion

Here, the swelling agent containing solvent/non-solvent (DMF/H$_2$O) with different proportions was used to treat the PVDF/CNT (rGO) blend membranes by a swelling and freeze-drying method. By varying three experimental parameters as DMF weight content in water, swelling time and freezing time, membrane surface and cross-section morphologies can be adjusted. The co-existence of both regular finger-like structure and dense sponge-like structure favors increasing adsorption capacity. Comparing with rGO/PVDF, CNT/PVDF blend membrane exhibited similar hydrophilicity and mechanical properties, however, better adsorption performance for MB dyes. The studies on the adsorption kinetics demonstrated that the adsorption process of CNT-based membranes is well fitted with the pseudo-first-order model, and the adsorption process of MB on the membrane is more consistent with the Freundlich isotherm model.

Acknowledgments

References

[1] J. Dasgupta, J. Sikder, S. Chakraborty, S. Curcio, E. Drioli, Remediation of textile effluents by membrane based treatment techniques: a state of the art review, J. Environ. Manage., 147 (2015) 55–72.

[2] R. Zhao, Y. Wang, X. Li, B. Sun, C. Wang, Synthesis of β-cyclodextrin-based electrospun nanofiber membranes for highly efficient adsorption and separation of methylene blue, ACS Appl. Mater. Interfaces, 7 (2015) 26649–26657.

[3] K. Yang, W. Wei, L. Qi, W.H. Wu, Q.F. Jing, D.H. Lin, Are engineered nanomaterials superior adsorbents for removal and pre-concentration of heavy metal cations from water?, RSC Adv., 4 (2014) 46122–46125.

[4] Mu. Naushad, G. Sharma, Z.A. Alothman, Photodegradation of toxic dye using Gum Arabic-crosslinked-poly(acrylamide)/ Ni(OH)₂/FeOOH nanocomposites hydrogel, J. Cleaner Prod., 241 (2019) 118263, doi: 10.1016/j.jclepro.2019.118263.

[5] G. Sharma, A. Kumar, Mu. Naushad, A. Kumar, A.H. Al-Muhtaseb, P. Dhiman, A.A. Ghfar, F.J. Stadler, M.R. Khan, Photoremediation of toxic dye from aqueous environment using monometallic and bimetallic quantum dots based nanocomposites, J. Cleaner Prod., 172 (2018) 2919–2930.

[6] Y. Xie, C. He, L. Liu, L. Mao, K. Wang, Q. Huang, M. Liu, Q. Wan, F. Deng, H. Huang, Carbon nanotube based polymer nanocomposites: biomimic preparation and organic dye adsorption applications, RSC Adv., 5 (2015) 82503–82512.

[7] S. Iijima, Helical microtubules of graphitic carbon, Nature, 354 (1991) 56–58.

[8] R.C. Haddon, Carbon nanotubes, Acc. Chem. Res., 35 (2010) 997–997.

[9] M. Kwon, Y. Hong, Flexible Temperature Sensor Array of PDMS-Encapsulated Conductive CNT Thin Films Fabricated by Solution Process, 2009 International Semiconductor Device Research Symposium, IEEE, College Park, MD, USA, 2009.

[10] A.E. Agboola, R.W. Pike, T.A. Hertwig, H.H. Lou, Conceptual design of carbon nanotube processes, Clean Technol. Environ. Policy, 9 (2007) 289–311.

[11] C. Baykasoglu, Z. Ozturk, M. Kirca, A.T. Celebi, A. Mugan, A.C. To, Effects of lithium doping on hydrogen storage properties of heat welded random CNT network structures, Int. J. Hydrogen Energy, 41 (2016) 8246–8255.

[12] D.-W. Jung, S. Park, S.-H. Kim, J.-B. Kim, E.-S. Oh, Durability of polymer electrolyte membrane fuel cell with Pt/CNTs catalysts in cell reversal conditions by hydrogen starvation, Fuel Cells, 11 (2015) 866–874.

[13] D.K. Yadav, S. Srivastava, Carbon nanotubes as adsorbent to remove heavy metal ion (Mn⁺⁷) in wastewater treatment, Mater. Today:. Proc., 4 (2017) 4089–4094.

[14] F. Yu, Y. Li, S. Han, J. Ma, Adsorptive removal of antibiotics from aqueous solution using carbon materials, Chemosphere, 153 (2016) 365–385.

[15] Y. Gao, Y. Li, L. Zhang, H. Huang, J. Hu, S.M. Shah, X. Su, Adsorption and removal of tetracycline antibiotics from aqueous solution by graphene oxide, J. Colloid Interface Sci., 368 (2012) 540–546.

[16] J. Suhartono, C. Tizaoui, Polyvinylidene fluoride membranes impregnated at optimised content of pristine and functionalised multi-walled carbon nanotubes for improved water permeation, solute rejection and mechanical properties, Sep. Purif. Technol., 154 (2015) 290–300.

[17] G.-d. Kang, Y.-m. Cao, Application and modification of poly(vinylidene fluoride) (PVDF) membranes – a review, J. Membr. Sci., 463 (2014) 145–165.

[18] F. Liu, N.A. Hashim, Y. Liu, M.R.M. Abed, K. Li, Progress in the production and modification of PVDF membranes, J. Membr. Sci., 375 (2011) 1–27.

[19] R.P.S. Chakradhar, G. Prasad, P. Bera, C. Anandan, Stable superhydrophobic coatings using PVDF – MWCNT nanocomposite, Appl. Surf. Sci., 301 (2014) 208–215.

[20] G.-E. Chen, L. Sun, Z.-L. Xu, H. Yang, H.-H. Huang, Y.-J. Liu, Surface modification of poly(vinylidene fluoride) membrane with hydrophilic and anti-fouling performance via a two-step polymerization, Korean J. Chem. Eng., 32 (2015) 2492–2500.

[21] S. Hong, S. Hua, L. Yan, Preparation and characterization of Al₂O₃/TiO₂/PVDF polymer composites ultrafiltration membrane, Appl. Mech. Mater., 253–255 (2013) 865–870.

[22] F.A. Sanchez, J. González-Benito, PVDFBaTiO₃/carbon nanotubes ternary nanocomposites: effect of nanofillers and processing, Polym. Compos., 38 (2015) 227–235.

[23] C. Zhao, X. Xu, J. Chen, F. Yang, Effect of graphene oxide concentration on the morphologies and antifouling properties of PVDF ultrafiltration membranes, J. Environ. Chem. Eng., 1 (2013) 349–354.

[24] M. Safarpour, A. Khataee, V. Vatanpour, Effect of reduced graphene oxide/TiO₂ nanocomposite with different molar ratios on the performance of PVDF ultrafiltration membranes, Sep. Purif. Technol., 140 (2015) 32–42.

[25] Y. Zhang, C. Jiang, R. Tian, G. Li, Hydrophilicity, pore structure and mechanical performance of CNT/PVDF materials affected by carboxyl contents in multi-walled carbon nanotubes, IOP Conf. Ser.: Mater. Sci. Eng., 284 (2018) 012009, doi: 10.1088/1757-899X/284/1/012009.

[26] S. Liang, G. Li, J. Zhang, R. Tian, Structuring of polystyrene surface via swelling–freezing drying in a binary solvent solution, J. Porous Mater., 22 (2015) 859–865.

[27] H. Liu, K. Nakagawa, D. Chaudhary, Y. Asakuma, M.O. Tadé, Freeze-dried macroporous foam prepared from chitosan/ xanthan gum/montmorillonite nanocomposites, Chem. Eng. Res. Des., 89 (2011) 2356–2364.

[28] P. Atorngitjawat, Effects of processing conditions and crystallization on dynamic relaxations in semicrystalline poly(vinylidene fluoride) films, Macromol. Res., 25 (2017) 391–399.

[29] Y.H. Li, Q.J. Du, T.H. Liu, X.J. Peng, J.J. Wang, J.K. Sun, Y.H. Wang, S.L. Wu, Z.H. Wang, Y.Z. Xia, L.H. Xia, Comparative study of methylene blue dye adsorption onto activated carbon, graphene oxide, and carbon nanotubes, Chem. Eng. Res. Des., 91 (2013) 361–368.

[30] J.-w. Li, X.-h. Xu, Non-isothermal crystallization of poly(vinylidenefluoride)/hollow glass microspheres composites, Polym. Plast. Technol. Eng., 51 (2012) 1204–1208.

[31] Y.L. Luo, W. Yu, F. Xu, Surface modification and vapor-induced response of poly(vinylidene fluoride)/carbon black composite conductive thin films, Polym. Plast. Technol. Eng., 50 (2011) 1084–1090.

[32] V. Garg, M. Amita, R. Kumar, R. Gupta, Basic dye (methylene blue) removal from simulated wastewater by adsorption using Indian Rosewood sawdust: a timber industry waste, Dyes Pigm., 63 (2004) 243–250.

[33] A. Gücek, S. Şener, S. Bilgen, M. Ali Mazmancı, Adsorption and kinetic studies of cationic and anionic dyes on pyrophyllite from aqueous solutions, J. Colloid Interface Sci., 286 (2005) 53–60.

[34] S. Banerjee, M.G. Dastidar, Use of jute processing wastes for treatment of wastewater contaminated with dye and other organics, Bioresour. Technol., 96 (2005) 1919–1928.

[35] W.T. Tsai, J.M. Yang, C.W. Lai, Y.H. Cheng, C.C. Lin, C.W. Yeh, Characterization and adsorption properties of eggshells and eggshell membrane, Bioresour. Technol., 97 (2006) 488–493.

[36] K. Legrouri, E. Khouya, M. Ezzine, H. Hannache, R. Denoyel, R. Pallier, R. Naslain, Production of activated carbon from a new precursor molasses by activation with sulphuric acid, J. Hazard. Mater., 118 (2005) 259–263.

[37] Y. Yao, H. Bing, X. Feifei, C. Xiaofeng, Equilibrium and kinetic studies of methyl orange adsorption on multiwalled carbon nanotubes, Chem. Eng. J., 170 (2011) 82–89.

[38] Mu. Naushad, A.A. Alqadami, Z.A. AlOthman, I.H. Alsohaimi, M.S. Algamdi, A.M. Aldawsari, Adsorption kinetics, isotherm and reusability studies for the removal of cationic dye from aqueous medium using arginine modified activated carbon, J. Mol. Liq., 293 (2019) 111442, doi: 10.1016/j.molliq.2019.111442.

[39] A.B. Albadarin, M.N. Collins, Mu. Naushad, S. Shirazian, G. Walker, C. Mangwandi, Activated lignin-chitosan extruded blends for efficient adsorption of methylene blue, Chem. Eng. J., 307 (2017) 264–272.

[40] A.A. Alqadami, Mu. Naushad, Z.A. Alothman, T. Ahamad, Adsorptive performance of MOF nanocomposite for methylene blue and malachite green dyes: kinetics, isotherm and mechanism, J. Environ. Manage., 223 (2018) 29–36.